Pergamon

0301-9322(94)E0023-C

Int. J. Multiphase Flow Vol. 20, No. 5, pp. 837–863, 1994
Copyright © 1994 Elsevier Science Ltd
Printed in Great Britain. All rights reserved
0301-9322/94 $7.00 + 0.00

SUBCOOLED VOID GROWTH MECHANISMS AND PREDICTION AT LOW PRESSURE AND LOW VELOCITY

E. L. BIBEAU and M. SALCUDEAN

Department of Mechanical Engineering, The University of British Columbia, Vancouver, B.C., Canada V6T 1Z4

(Received 30 April 1993; in revised form 15 March 1994)

Abstract—Measurements were made of void growth and wall temperatures for two circular annular geometries and forced-convective subcooled nucleate boiling conditions, with flow rates between 0.02 and 0.20 kg/s, pressures of 1.05, 2 and 3 bar, and inlet temperatures between 30 and 90°C. Void growth results at low pressure show that the highly subcooled void region is important, and void fraction at the onset of significant void may be as high as 10%. Observations of bubble ebullition and detachment mechanisms obtained from a high speed photographic study were compared to assumptions generally used in void growth modeling. The photographic results show that bubbles do not travel far downstream after nucleating, that there is no region of attached void and that bubbles slide along the wall before being ejected into the flow after the onset of nucleate boiling. Unlike findings for high pressure systems reported in the literature, the onset of significant void was found to be independent of (i) bubble detachment, (ii) the location where the bubble is first ejected from a bubble layer and (iii) the transition from partial nucleate boiling to fully developed boiling. A phenomenological void growth model is presented which accounts for the vapor volume inside a heated channel at atmospheric pressure, and includes the bubble ebullition cycle, formulated on the basis of information obtained from the high speed photographic study.

Key Words: void fraction, subcooled, nucleate boiling, bubble, void growth modeling, bubble detachment, growth rate, high speed photography

1. INTRODUCTION

During subcooled boiling, the fluid bulk temperature is lower than the saturation temperature, and boiling occurs on a heated surface, thus producing "void". Understanding void growth in subcooled boiling conditions is important in the design of two-phase flow heat transfer equipment such as boilers and heat exchangers. Void formation controls power excursions for pool-type nuclear reactors such as the SLOWPOKE (Hilborn *et al.* 1972) and MAPLE (Lidstone & Saroudis 1986) reactors. These reactors operate at near atmospheric pressure. Void is assumed to act as a main mechanism for controlling power excursions during postulated upset conditions. The prediction of void growth is required to calculate the reactivity of the core in the safety analysis of these reactors.

An experimental program has been established to study void growth during upset conditions which might occur in the SLOWPOKE and the MAPLE reactors for conditions of low pressure (1–3 bar) and low velocity (0.08–1.2 m/s). Bubble ebullition and bubble detachment mechanisms must be properly understood in order to develop a phenomenological void growth model for these conditions.

Assumptions from previous void growth models, developed mainly for high pressure applications, are reviewed and then evaluated, and their validity is examined based on void growth measurements and high speed photographic results obtained for low pressure and low velocity conditions. A phenomenological void growth model is developed based on the experimental findings.

2. BACKGROUND

2.1. Void growth

Figure 1 shows the temperature, void fraction and bubble layer development along a uniformly heated channel, as currently portrayed in the literature (Serizawa & Kenning 1979). As the

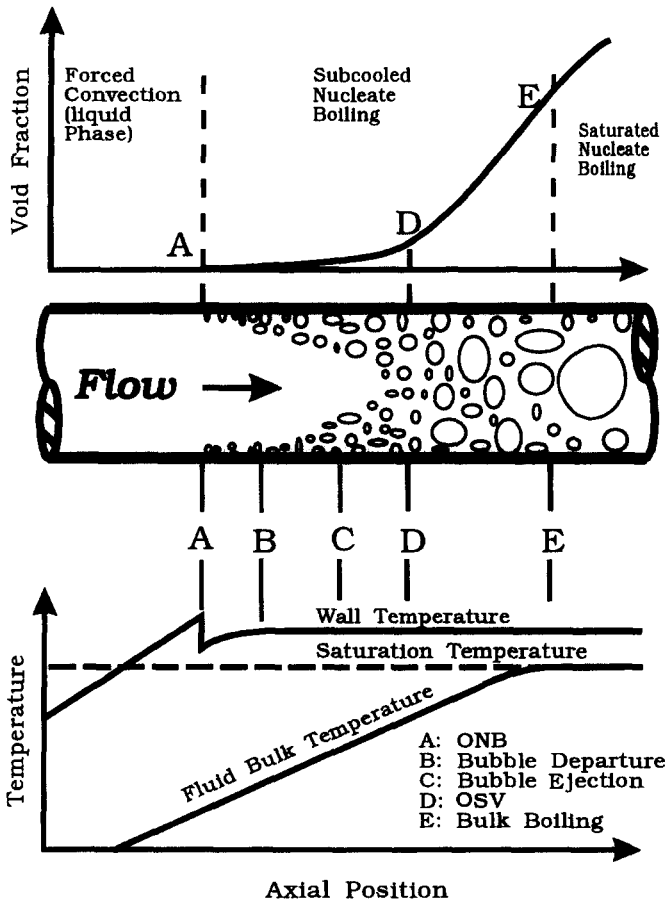

Figure 1. Void fraction and wall temperature along a uniformly heated channel.

subcooled liquid enters the channel, both the bulk and the wall temperature increase linearly upstream of point A. Point A is referred to as the onset of nucleate boiling, or ONB, which occurs when the wall temperature exceeds the saturation temperature by a certain amount, and bubbles begin to nucleate on the heated surface. The density of nucleation sites increases downstream from point A. Vapor bubbles remain attached to the heated wall up to point B, which corresponds to the bubble detachment point. The bubbles slide along the wall downstream of this point, and the bubble layer grows until the first bubble is ejected into the core of the flow at point C. The onset of significant void, or OSV, occurs at point D, and is characterized by a rapid increase in the slope of the void growth curve. Finally, the fluid reaches saturation at point E.

The characteristic heat transfer regimes are also shown in figure 1. Single-phase forced-convection heat transfer occurs before point A, subcooled nucleate boiling occurs in the region between points A and E, and saturated nucleate boiling occurs after point E.

Several mechanisms have been proposed to explain how the heat is transferred from the heated wall to the flowing liquid during nucleate boiling. The heat may be transferred by single-phase convection between the patches of bubbles in the partial nucleate boiling region (Rouhani 1968; Lahey 1978), by the latent heat of bubbles (Chang 1963; Lahey 1978; Rouhani 1968), by condensation at the top of the bubbles while the bubbles are still attached to the heated wall (Chang 1963; Unal 1976), by micro-convection due to bubble agitation in the fluid (Hsu & Graham 1961; Lahey 1978; Chang 1963; Rohsenow & Clark 1951), or by transient conduction, which heats the cold fluid replacing departing bubbles between successive periods of bubble growth (Rouhani 1968; Hsu & Graham 1961).

2.2. *Assumptions in void growth models*

Many researchers (e.g. Levy 1967; Bowring 1962) have investigated void growth mainly at high pressure, due to its importance to the nuclear and chemical industries. In most investigations, the void growth curve is separated into two regions:

(1) *A highly subcooled region* (region A–D in figure 1). This region is defined as the attached void region where the liquid temperature near the wall is sufficiently high to permit the formation of small bubbles. These bubbles either remain attached to the wall, or slide along the wall and condense very rapidly. Most of the heat within this region is used to raise the liquid bulk temperature.

(2) *A low subcooled region* (region D–E in figure 1). In this region, void fraction increases rapidly as the subcooling decreases. Bubbles survive in the liquid core.

In line with present practice, the transition point between both regions is defined as the onset of significant void, or OSV (point D in figure 1). Prediction of void growth using previous models requires an accurate determination of the OSV. Most void growth models assume that the OSV occurs either at the location where the bubbles first detach from the heated wall (Rouhani 1968; Levy 1967; Bowring 1962; Ahmad 1970; Staub 1968; Saha & Zuber 1974; Larsen & Tong 1969; Rogers *et al.* 1987; Chatoorgoon 1992), or where the bubbles first eject from the detached bubble layer (Serizawa & Kenning 1979; Lahey 1978), or at the transition from partial nucleate boiling to fully developed nucleate boiling (Griffith *et al.* 1958).

Models which relate the OSV to the location where the bubble first detaches assume that bubbles grow and collapse on the wall in the highly subcooled region. These models either assume that the bubbles do not slide before the OSV (Levy 1967; Bowring 1962; Ahmad 1970; Staub 1968), or that they may slide on the wall before the OSV (Rouhani 1968; Larsen & Tong 1969; Rogers *et al.* 1987; Chatoorgoon 1992). Bowring (1962) was the first to relate the OSV to bubble detachment at high pressure, but this assumption was not verified by photographic studies. Saha & Zuber (1974) assumed that the OSV was governed by bubble detachment for Peclet numbers greater than 70,000. Chatoorgoon (1992) assumed that bubbles were attached to the wall before the OSV, but the authors were aware that this assumption might not be valid, based on experimental findings by Dix (1971), who observed that bubbles were detached from the wall before the OSV for pressures between 3.1 and 8.4 bar.

Models which relate the OSV to the location where the bubbles are first ejected from a bubble layer (Serizawa & Kenning 1979; Lahey 1978) assume that bubbles are detached from the wall and travel in a bubble layer close to the wall in the highly subcooled region. Based on the photographic study by Dix (1971), these models assume that the bubbles are ejected into the liquid core at the OSV when they are no longer stable inside the layer.

Saha & Zuber (1974) proposed a thermally-controlled model for low Peclet numbers where the Nusselt number was assumed constant at the OSV, with the OSV not being governed by bubble detachment. Void growth measurements for four annular geometries by Bibeau *et al.* (1993) have shown that the Nusselt number is not a constant at the OSV, but varies with the ratio of the hydraulic diameter to the heated surface area.

Table 1 shows several void growth models, their corresponding range of application, and gives a brief description of the assumptions on which the prediction of the OSV is based.

2.3. *Bubble detachment*

In void growth studies, bubble detachment is assumed to be caused by static forces parallel to the heated wall (Levy 1967; Staub 1968; Rogers *et al.* 1987). Bubble radius at departure is determined by balancing the hydrodynamic drag, buoyancy and surface tension forces on a single bubble, as shown in figure 2(a). The forces normal to the heated wall are assumed to be small compared to the forces parallel to the wall.

3. OVERVIEW OF VOID GROWTH MODELING

There is no reliable evidence in the literature showing that bubbles detach from the wall near the OSV at low pressure. Flow visualization with the naked eye supports the concept that bubbles

Table 1. Range of applicability of void growth models

Models	P (bar)	ϕ (MW/m^2)	G (kg/m^2 s)
OSV governed by detachment; no sliding before detachment			
Bowring (1962)	1–140	0.02–2.00	100–2000
Levy (1967)	19–50	0.60–1.20	130–1450
Staub (1968)	1–140	0.02–2.00	30–2000
Ahmad (1970)	10–130	0.30–1.20	130–1450
Saha & Zuber (1974)	1–49	0.02–1.21	400–1050
OSV governed by detachment; sliding before detachment			
Rouhani (1968)	19–138	0.18–1.20	130–9100
Larsen & Tong (1969)	14–140	0.60–1.20	3300
Rogers *et al.* (1987)	1.5	0.30–1.20	70–450
Chatoorgoon (1992)	1.5–2.1	0.50–1.16	315–420
OSV governed by eject from layer			
Lahey (1978)	19–50	0.60–1.20	130–1450
Serizawa & Kenning (1979)	1–158	0.23–1.66	130–2100
OSV governed by transition to fully developed boiling			
Griffith *et al.* (1958)	34–102	0.18–1.20	6000–9000

"seem" to be attached to the wall before the OSV (Bibeau 1993), but this method of visualization cannot provide sound experimental evidence of bubble behavior, since bubbles grow and collapse within a few milliseconds (Gunther 1951). High speed photography appears to be the only method for providing detailed visual observations of the bubble ebullition.

Salcudean & Bibeau (1991) and Bibeau & Salcudean (1990) obtained experimental evidence showing that the OSV is not governed by bubble detachment at low pressure. Experimental data for void growth for upward and downward flow showed that bubble detachment occurs at higher subcooling for downward flow than for upward flow. If the OSV was determined solely by bubble detachment, it would occur at lower subcooling for downward flow. The reason for this is that, for downward flow, the buoyancy force acts in the opposite direction to the hydrodynamic force, thus delaying the bubble departure [figure 2(b)].

At high pressure, Unal (1975) and Dix (1971) found photographic evidence showing bubbles detaching before the OSV, which indicates that bubble detachment is not related to the OSV.

The assumption that bubbles do not slide in the highly subcooled region (Levy 1967; Bowring 1962; Ahmad 1970; Staub 1968) contradicts photographic studies which report a bubble slip ratio of approximately 0.8 (Gunther 1951; Akiyama & Tachibana 1974).

Bubble detachment models based on a force balance parallel to the wall (Levy 1967; Staub 1968; Rogers *et al.* 1987) cannot explain why a bubble which detaches due to forces parallel to the wall

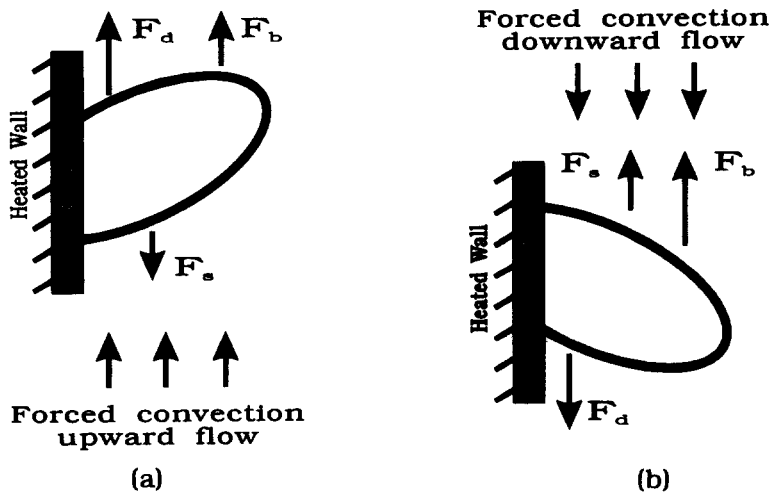

Figure 2. Bubble detachment force balance for (a) upward flow and (b) downward flow, where F_d = drag force, F_b = buoyancy force and F_s = surface tension force.

is propelled into the core of the flow. These models assume that forces normal to the wall are negligible compared with the forces parallel to the wall. The influence of forces normal to the wall has never been addressed in void growth studies.

In order to verify previous void growth assumptions, and to clarify the mechanism of void growth, void growth measurements and a high speed photographic study were performed. A previous void growth investigation by Salcudean & Bibeau (1991) showed that the highly subcooled region (AD from figure 1) is larger at low pressure than at high pressure, making it possible to obtain a detailed description of bubble behavior in this region. The high speed photographic results are only briefly reported since a detailed presentation can be found in Bibeau & Salcudean (1994).

4. EXPERIMENTAL FACILITY

4.1. Two-phase flow loop

Figure 3 is a schematic diagram of the experimental two-phase loop used for the present void growth experiments and bubble visualization studies. Using the closed-loop system, a forced-convective flow is generated past a circular element inside an annulus. This simulates the flow conditions (pressure, inlet temperature and velocity) expected during certain postulated upset conditions in the reactor. The closed-loop system consists of the following components: main pump, immersion heater, filter, turbine flow metering system, flow control valve, heated test section, vertical cross-flow condenser and heat exchanger. A recirculating system, consisting of a pump connected to a storage tank, as shown in figure 3, generates a constant pressure at the outlet of the test section, regardless of the conditions within the test loop. The loop is filled with distilled water, and air bleed valves are used to remove the trapped air.

The vertical test section consists of a circular heater, which is electrically heated by a 64 kW AC low voltage power supply, and an outer Pyrex glass tube. Two test sections were used: a small circular test section C-s, and a large circular test section C-l, both shown in figure 4. Test section C-s was fabricated and instrumented with three wall temperature thermocouples by Atomic Energy of Canada Limited (Kowalski *et al.* 1988). The circular heater for test section C-s is a stainless steel rod 9.53 mm in diameter and 600 mm in length; the circular heater for test section C-l is fabricated

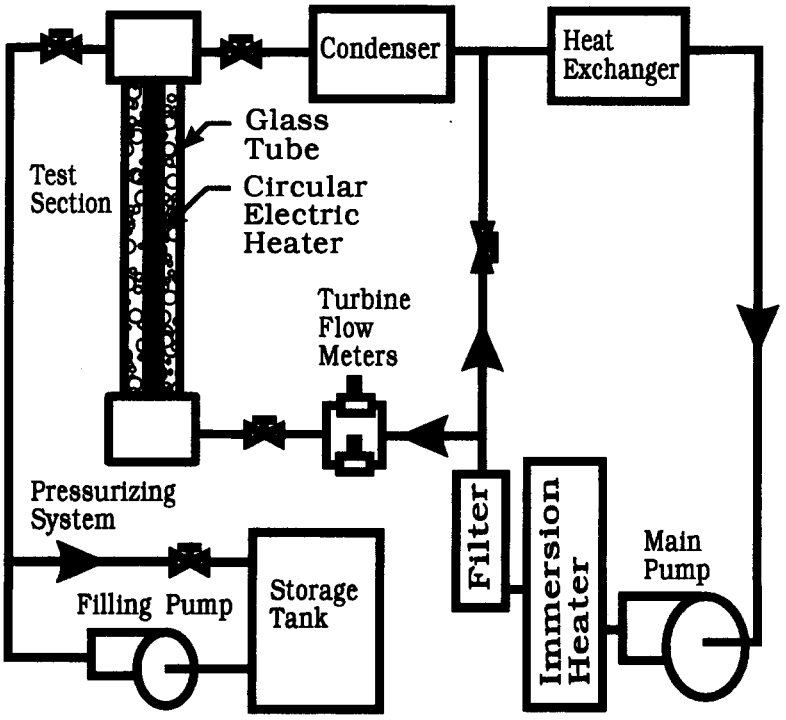

Figure 3. Schematic diagram of the two-phase flow loop.

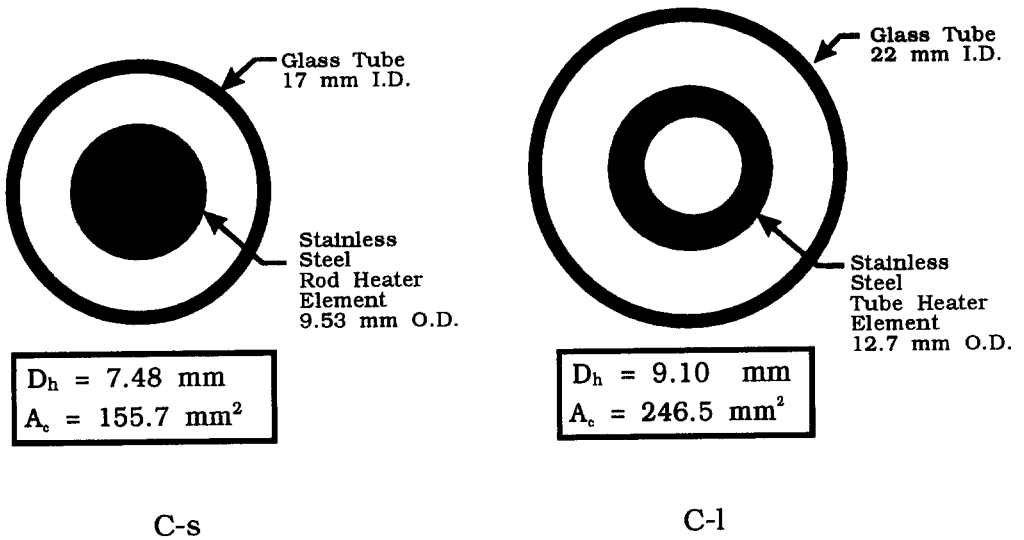

Figure 4. The two annular test sections used in this study.

from a 12.7 mm stainless tube that is 2.2 mm thick and 480 mm in length. Both heaters were polished with #400 emery paper and silver-welded at both ends to thick-wall copper or brass tubes. The inner diameter of the glass tube for test sections C-l and C-s is 22 and 17 mm, respectively. The diameter and length of the heater for test section C-l are identical to an actual fuel element used in the SLOWPOKE reactor. The diameter of the circular heater for test section C-s was chosen to obtain a characteristic hydraulic diameter representing a non-finned heater for the MAPLE reactor.

4.2. Instrumentation

Void growth was measured using a gamma-ray densitometer at an axial location of 440 mm for test section C-l, and 550 mm for test section C-s. The gamma-ray densitometer operates on the principle of differential absorption of gamma rays in water versus water vapor. The gamma-ray densitometer, as shown in figure 5, uses a 10 mCi cobalt-57 source with a NaI (Tl) 50 mm diameter scintillator, a ten-stage photomultiplier and a counter system consisting of a spectroscopy amplifier, spectrum stabilizer and a signal channel analyzer. Void fraction is determined by:

$$\epsilon = \frac{\ln(F_w/F)}{\ln(F_w/F_a)} \qquad [1]$$

where F_w and F_a are the calibration frequency values when the annulus is filled with water and air, respectively, and F is the measured frequency. Typical values for F_w and F_a are 11,000 and 18,000 Hz, respectively.

Wall temperatures for test section C-s were measured with special grade chromel/alumel thermocouple wire at three axial locations: 135, 335 and 550 mm. The 0.1 mm diameter wires were spot-welded on the surface of the heater. The measurement error, shown in table 4 and described in Bibeau (1993), includes errors due to the sensor, the calibration and conduction along the wire. Wall temperature measurements for test section C-l were reported in Bibeau (1988).

Static pressure at the outlet was monitored with a Bourdon pressure gauge. The current and the voltage drop measurements obtained across the heater were used for the heat flux calculation, and the inlet and outlet temperatures were measured with K-type ungrounded thermocouples.

The instrumentation was interfaced to a high speed analog/digital board connected to a 486 IBM compatible computer. An interactive data acquisition program calibrated the instrumentation, recorded the measurements, displayed the results graphically while an experiment was conducted, and controlled the various experimental components: pumps, immersion heaters, flow rate, power level and cooling flow rate to the condenser. More information on the experimental apparatus is given in Bibeau (1993).

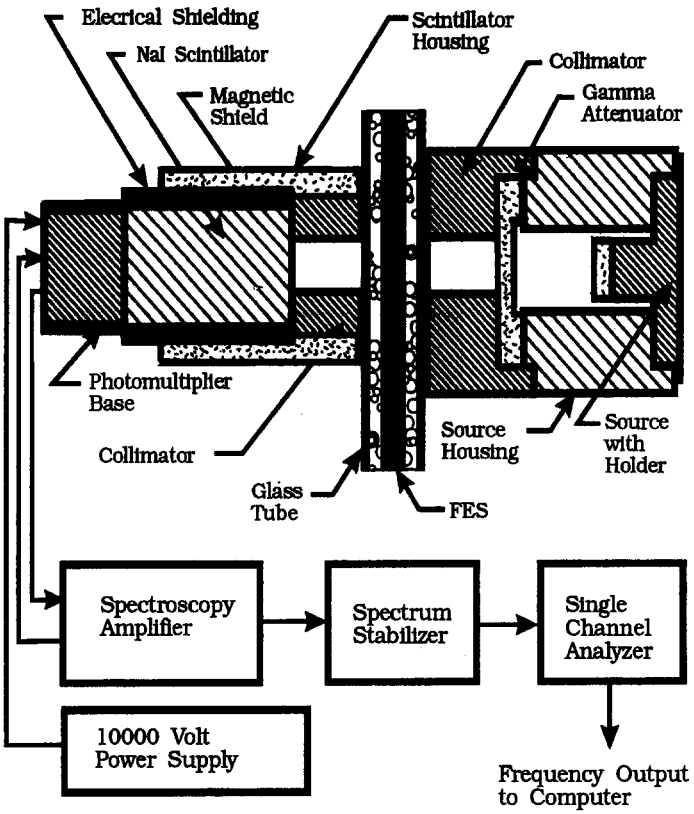

Figure 5. Gamma-ray densitometer assembly drawing and counter system.

4.3. *Input parameters for void fraction measurements*

Forty-eight void fraction experiments were carried out for each test section with constant inlet temperature, outlet pressure and flow rate by varying the heat flux from 0 to a value which produced more than 30% void inside the test section. In this manner, measurements were obtained in both the single phase forced-convection region and the boiling region. The ONB was visually recorded, and the OSV was calculated based on the intersections of two least squares lines, as detailed in section 4.4. The values of inlet temperature, flow rate, and pressure are shown in table 2. Each experiment is composed of 30–70 data points, with each point being a measurement of void fraction, wall temperatures, flow rate, inlet and outlet temperatures, current and voltage drop across the heater.

4.4. *Determination of the onset of significant void*

The OSV is usually determined graphically at the point where the slope of the void growth curve changes abruptly. A more accurate method is introduced in figure 6. A point j is selected where

Table 2. Variation of parameters for the two test sections

Input experimental parameters		
$\dot{m}$ (kg/s)	0.02, 0.05, 0.10, 0.15, 0.20	
P (bar)	1.1, 2.0, 3.0	
T_{in} (°C)	30.0, 45.0, 60.0, 75.0, 90.0	
Test section dependent parameters		
	C-s	C-l
D_h (mm)	7.5	9.1
A_c (mm^2)	155.7	246.6
U (m/s)	0.13–1.3	0.08–0.84
Pe	5600–56,000	4600–46,000

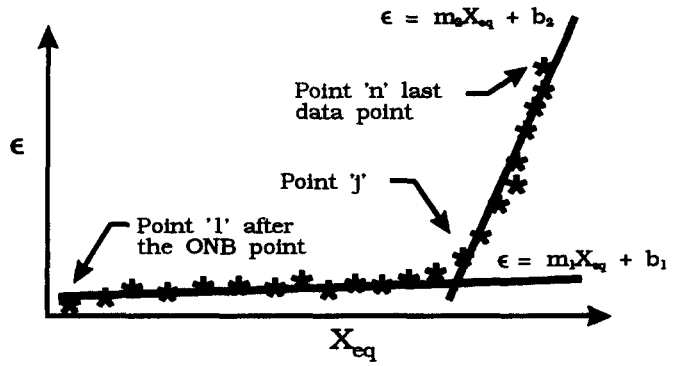

Figure 6. Determination of the onset of significant void.

there is a rapid change in the slope of the void growth curve (initial OSV guess). Two lines are determined from a least-square-fit: a line $\epsilon = m_1 X_{eq} + b_1$, using the experimental data points from 1 (first point after ONB) to j, and a line $\epsilon = m_2 X_{eq} + b_2$, using the experimental data points from $j + 1$ to n (last data point). The experimental data point which is closest to the intersection of the two lines is the OSV. This method is relatively independent of the initial OSV guess.

4.5. High speed photography

High speed photography (5000–6000 frames per second) at atmospheric pressure was performed using a Hycam at the same location where void fraction was measured for test section C-1 ($l = 440$ mm). Figure 7 shows the experimental setup. An 8 mm section of the annular flow passage

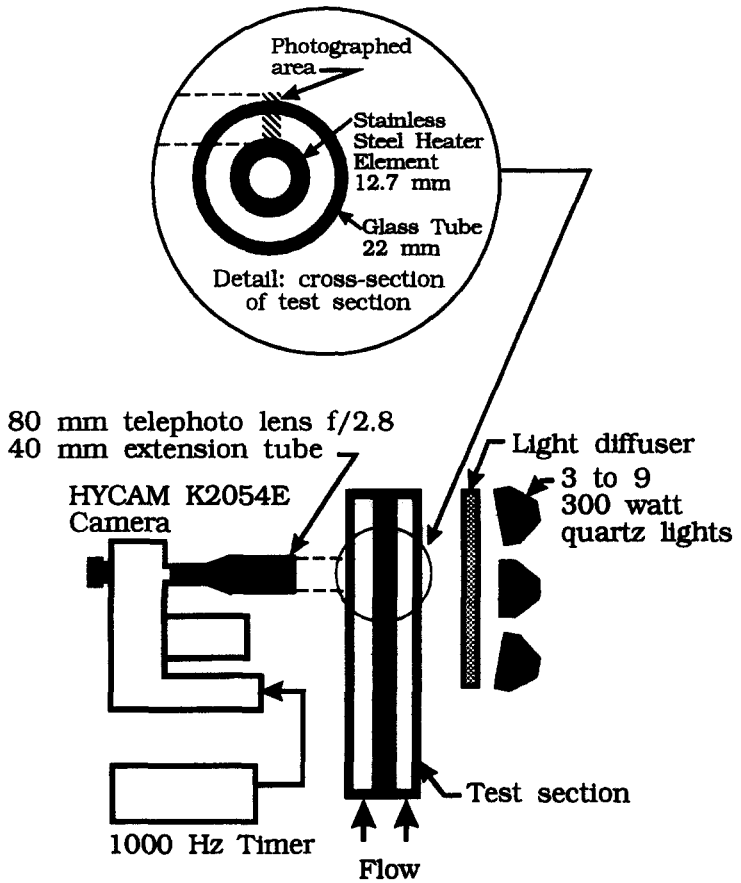

Figure 7. High speed photography experimental setup.

from the heater to the glass tube is filmed on each frame. Encoded on the high speed film is a constant frequency time mark of 1000 Hz; the high speed camera imprints a fixed reference mark on each frame. The film is converted into a video signal using a solid state CCD camera system which enlarges the image up to 36×. Each image is digitized using a 640 × 480 frame grabber.

An interactive computer developed by Farajisarir (1993) was used to process the digitized image. For each bubble ebullition cycle, the outlines of 20–40 bubbles were traced with a mouse on the computer screen. The parameters measured for each bubble presented in this paper are (figure 8): the parallel displacement of the center of the bubble with respect to the nucleation site, L_p; the normal displacement of the center of the bubble with respect to the wall, L_n; the real time obtained from the time coded film, t; the bubble volume, V_b; and the bubble volume equivalent radius, R_b. The bubble volume is obtained by averaging two volumes, which are calculated as follows: the two areas located on each side of the minimum axis of inertia (figure 8) are revolved separately about the axis, thus creating two bodies of revolution. Their volumes are then averaged to obtain V_b. The volume equivalent radius is by definition:

$$R_b = \left(\frac{3V_b}{4\pi}\right)^{1/3} \quad [2]$$

The reference mark on each photographic frame is used to measure accurately the displacement of the center of mass of the bubble. The accuracy of the measured parameters is shown in table 4 and detailed in Farajisarir (1993).

More than 50 high speed photographic films were obtained for the various values of heat flux, subcooling and flow rate listed in table 3.

A detailed description of the photographic study can be found in Farajisarir (1993).

4.6. Experimental procedure

The distilled loop water was changed every 3 days, and was heated to 100°C prior to an experiment to de-gas the water. The trapped air in the condenser or the immersion heater was removed periodically.

For void fraction measurements, the void meter was calibrated before every experiment. The inlet temperature, outlet pressure and flow rate were set accordingly. The heat flux was increased by the computer, and sufficient time was allowed for the flow conditions inside the annulus to reach a steady state before measurements were taken. Void fraction was measured after the ONB, and the measurements were averaged over a 70 s time interval. The heat balance across the test section was verified by comparing the outlet temperature calculated from a heat balance to the measured outlet temperature. The temperature difference had to be less than 2.0°C for the heat balance to be considered acceptable. At the conclusion of an experiment, void fraction was measured with only water in the annulus to verify the void meter calibration.

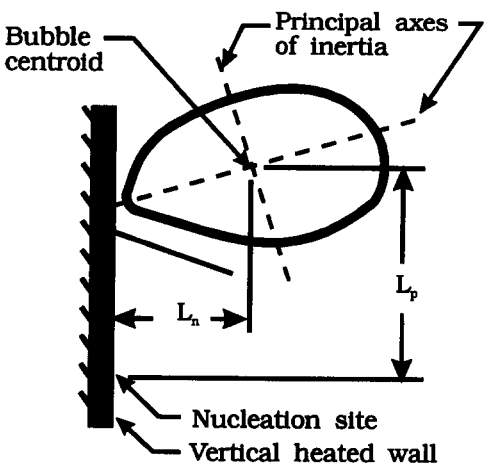

Figure 8. Bubble parameters measured from the digitized image.

Table 3. Input parameters for high speed photographic study

Input parameter	Range
T_{sub} (°C)	10, 20, 30, 40, 60
$\dot{m}$ (kg/s)	0.02, 0.10, 0.20
ϕ (MW/m^2)	0.1–1.2
P (bar)	1.05

Table 4. Estimated error for experimental parameters

Parameter	Error (±)
Void, ϵ	3% void
Wall temperature, T_{1-3}	2.3°C
Inlet pressure, P	140 Pa
Inlet temperature, T_{in}	1.0°C
Flow rate, $\dot{m}$	0.3%
Heat flux, ϕ	1.8%
Parallel displacement, L_p	0.1 mm
Normal displacement, L_n	0.1 mm
Time, t	0.02 ms
Bubble equivalent radius, R_b	1.6%
Bubble volume, V_b	5.0%

For high speed photography, the inlet temperature, flow rate and heat flux were adjusted until the desired subcooling was achieved. The quartz lights were then turned on, and the high speed camera activated. The wall temperature and flow conditions were measured simultaneously, and all photographic films were obtained using the same heater at the same camera location. Only bubbles produced at the same active nucleation site were digitized, and five to ten bubbles were digitized from each film.

4.7. Error analysis

Table 4 shows the experimental errors. Errors for directly measurable quantities were either obtained from specifications provided by the manufacturer, or estimated from experiments and calibration. For calculated parameters, the error was estimated using the error propagation method. The error analysis for the gamma-ray densitometer is discussed in Bibeau *et al.* (1993).

Additional information on the experimental facility can also be found in Bibeau (1993).

5. RESULTS AND DISCUSSION

Experimental results obtained at low pressure are presented and discussed in the following section, with special emphasis on their implications for the validity of previous void growth assumptions.

5.1. Wall temperature results

Figure 9 shows the void growth and wall temperature experimental results for test section C-s at a pressure of 2 bar, an inlet temperature of 30°C and a flow rate of 0.02 kg/s. The results are

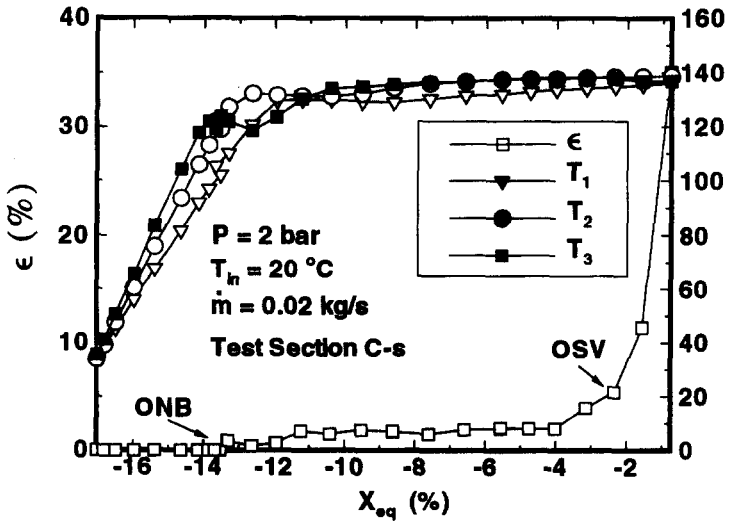

Figure 9. Void growth and wall temperatures for test section C-s.

scaled with respect to the equilibrium quality, X_{eq}, and evaluated at $l = 550$ mm, the location where void fraction and wall temperature T_3 are measured. T_1 and T_2 correspond to the wall temperatures at an axial location of 135 and 335 mm, respectively. The onset of nucleate boiling shown in the figure corresponds to the visually observed location of $l = 335$ mm, where the first bubbles were seen to nucleate.

The wall temperature measurements show the three heat transfer regions: single-phase forced-convection (the segment where wall temperature increases linearly with equilibrium quality); partial nucleate boiling (the segment where wall temperature first decreases and then stabilizes); and fully developed nucleate boiling (the segment where wall temperature is relatively independent of equilibrium quality). The void fraction increases slowly in the highly subcooled region, which is defined as the region between the onset of nucleate boiling and the OSV. After the OSV, the void fraction increases rapidly.

Figure 9 shows that the OSV occurs in the region where the wall temperature is relatively insensitive to changes in heat flux, i.e. in the fully developed boiling region. The results, therefore, show that, at low velocity, the OSV does not occur at the transition between partial nucleate boiling and fully developed boiling, as stated in previous void growth models (Lahey 1978; Griffith *et al.* 1958). At high flow rates (0.20 kg/s) and high inlet temperatures (75 and 90°C), the highly subcooled region is comparatively short, and the OSV is found to occur closer to the transition between partial nucleate boiling and fully developed boiling, but never at the transition.

5.2. Void growth results

Figure 10 shows an example of the void growth results for test section C-s, scaled by the equilibrium quality, for pressures of 1.1, 2.0 and 3.0 bar, $T_{in} = 30$, 45, 60 and 75°C, and the lowest tested flow rate: $\dot{m} = 0.02$ kg/s. The figure shows that void growth can be represented by a single curve when scaled with X_{eq} for different values of pressure. Similar void growth behavior is observed when void growth curves are scaled with the inlet temperature for $\dot{m} = 0.02$ kg/s. The figure shows that the OSV occurs close to saturation conditions at this low flow rate, indicating better mixing inside the test section when approaching pool boiling conditions ($\dot{m} \rightarrow 0$). The increase in mixing is produced by the more vigorous stirring of the bubbles, which are subjected to a smaller force by the cross flow rate (0.02 kg/s).

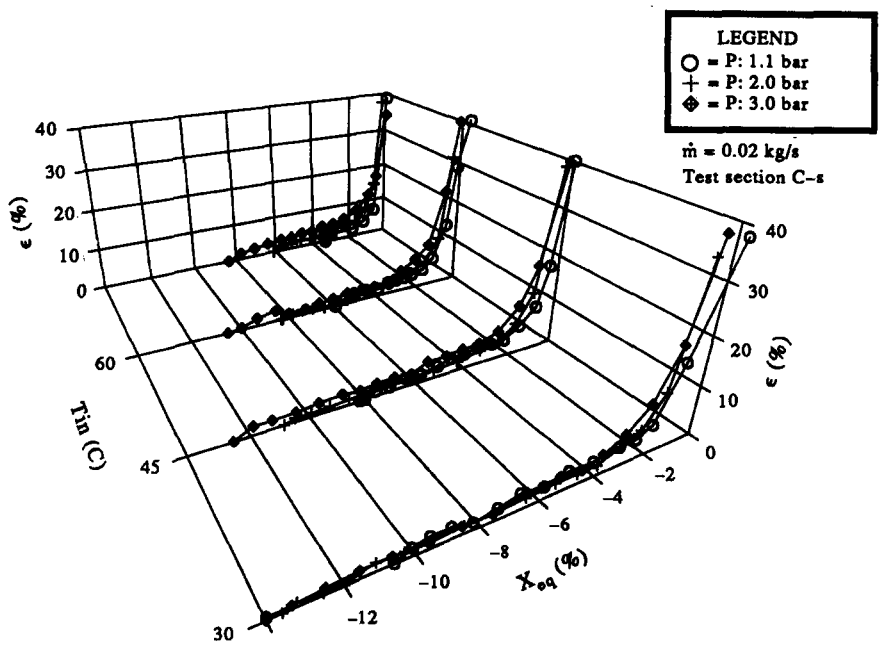

Figure 10. Influence of pressure on void growth for test section C-s at low flow rate and scaled with equilibrium quality.

Figure 11 shows void growth experiments for test section C-1 for flow rates of 0.02 and 0.20 kg/s. Results are scaled with the modified equilibrium quality X^*_{osv}, defined by the authors as:

$$X^*_{osv} = \frac{h_f - h}{h_f - h_{osv}} \quad [3]$$

where

h_f = enthalpy of saturated liquid (J/kg °C)
h = enthalpy of liquid (J/kg °C).

This parameter is the ratio of the local subcooling to the subcooling at the onset of significant void. The highly subcooled region is between $1 < X^*_{osv} < 7$, the OSV is at $X^*_{osv} = 1$ and the exponential region is between $0 < X^*_{osv} < 1$. For $\dot{m} = 0.02$ kg/s, the highly subcooled region is much longer than for $\dot{m} = 0.20$ kg/s, and the void fraction at the OSV is approximately 10%. At a flow rate of 0.20 kg/s, the highly subcooled region becomes shorter and the void fraction at the OSV decreases. The figure shows that a large majority of the void fraction data is obtained in the highly subcooled region. Many void growth models assume that the void fraction before the OSV is negligible, e.g. Levy (1967), and, therefore, the highly subcooled region shown in the figure is usually not taken into account. The present results indicate that a phenomenological void growth model at low values of velocity and pressure must account for void generated in the highly subcooled region.

The influence of pressure, flow rate and power on void growth for these experiments is discussed in Bibeau (1993).

5.3. *Bubble behavior*

High speed photographic films were taken in the highly subcooled region, at OSV and after OSV, for conditions listed in table 3. Typical bubble behavior in the highly subcooled region is shown in figure 12 for $T_{sub} = 10°C$, $\dot{m} = 0.10$ kg/s and $\phi = 0.3$ MW/m^2. The digitized results of the bubble history illustrated in figure 12 are shown in figure 13: the volume, V_b, the volume equivalent radius, R_b, and the displacement of the center of mass of the bubble parallel to the heater, L_p, and normal to the heater, L_n^* (L_n minus L_n at ejection).

Figure 12 shows a typical bubble which grows rapidly, subsequently elongates in the direction normal to the heater, and is then ejected into the flow where it condenses rapidly. At ejection, the bubble resembles an inverted pear with the stem touching the wall, as shown in the figure at $t = 6.6$ ms.

Figure 13 shows that the bubble slides almost immediately upon nucleation by a positive amount, L_p. The average bubble slip ratio [bubble sliding velocity (u_b)/mean flow velocity (U)] is the slope

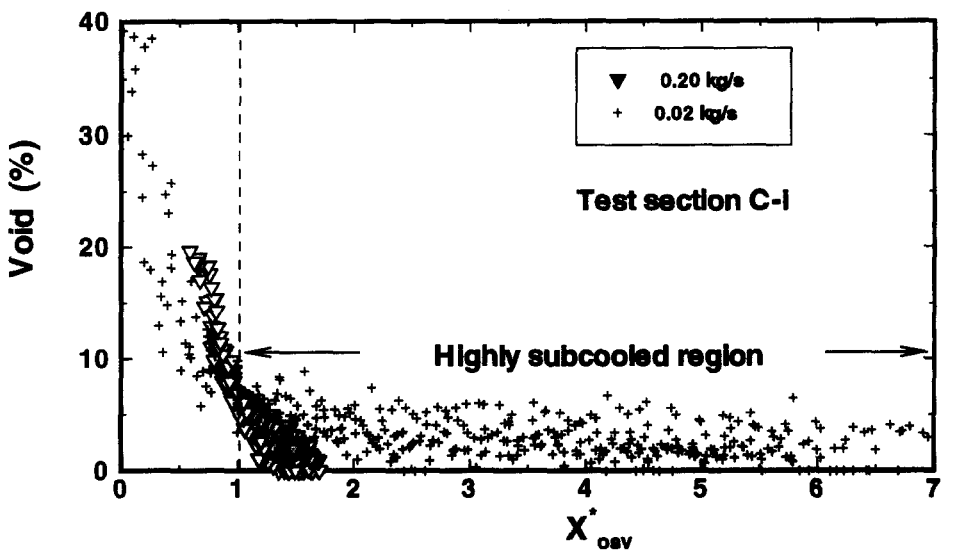

Figure 11. Void growth for test section C-1 and scaled with X^*_{osv}.

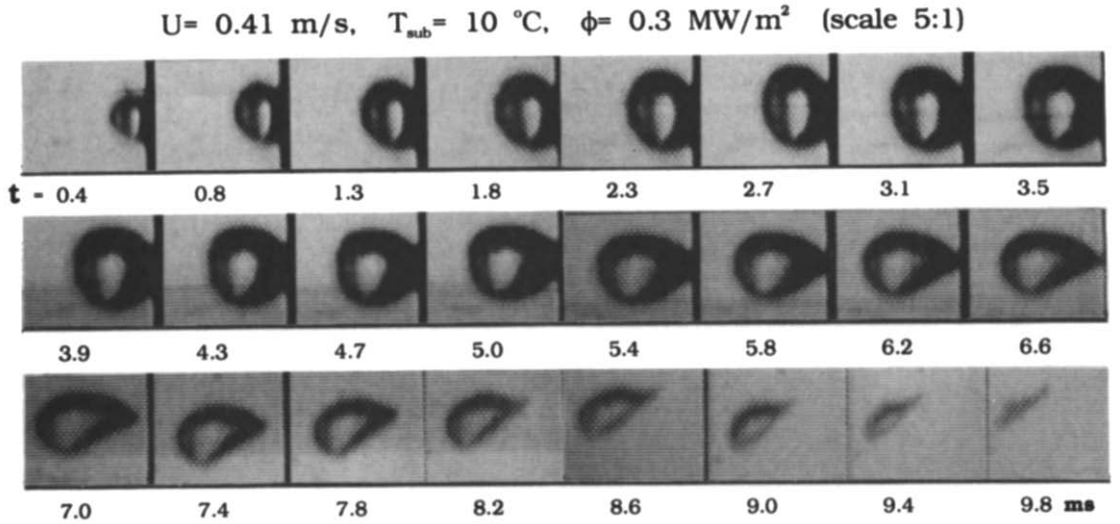

Figure 12. Bubble ebullition cycle in the highly subcooled region.

of the parallel displacement, L_p, before ejection and is equal to 1.2. After reaching a maximum radius, the bubble condenses considerably while sliding on the wall before ejecting into the flow. The bubble volume decreases significantly in this region.

The bubble ebullition cycle is divided into the sliding phase and the ejection phase, as shown in the figure. The authors introduce two terms: "parallel detachment", which refers to the location where the bubble starts to slide along the wall, and "normal detachment", which refers to the location where the bubble ejects into the flow. In Bibeau (1993), it is shown that the bubble radius at parallel detachment can be modeled using a static force balance parallel to the heated wall. At normal detachment, it is shown that the usually-considered dynamic forces are small since the bubble has stopped growing, as shown in figure 13, and, therefore, normal detachment must be controlled by forces which depend on the temperature gradient at the wall.

The models in table 1, which assume that the bubble does not slide in the highly subcooled region, do not represent the true physical phenomenon. For conditions investigated in table 3, all bubbles were found to slide after nucleation. The slip ratio, therefore, is not equal to zero in the highly subcooled region, as is often assumed in void growth models (Levy 1967).

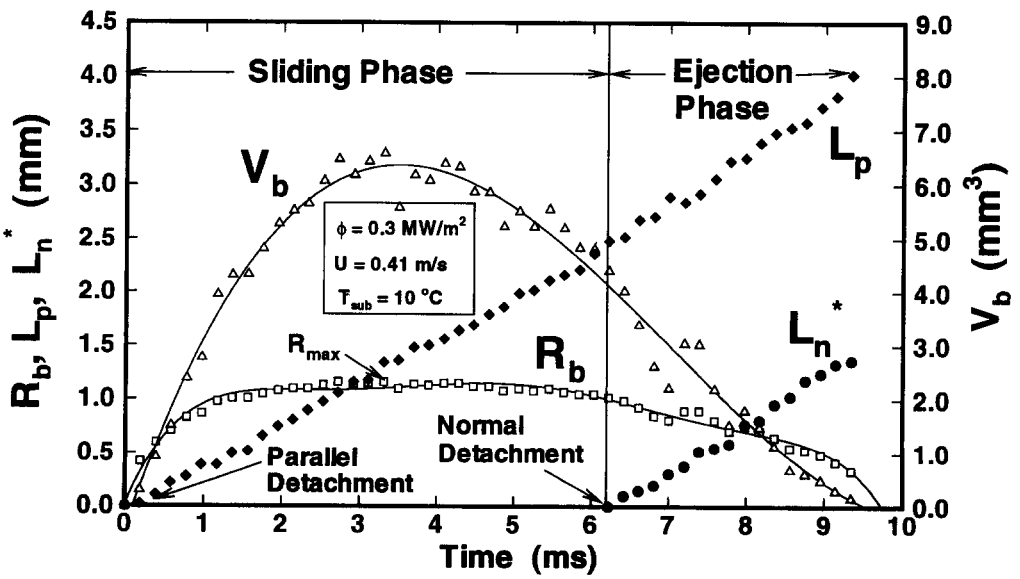

Figure 13. Bubble volume, bubble volume equivalent radius and displacement of center of mass of the bubble with respect to the nucleation site and the heated wall.

In addition, many void growth models assume that the bubbles grow and collapse on the heater in the highly subcooled region (Staub 1968; Rogers *et al.* 1987). High speed photography reveals that, for subcoolings between 10 and 60°C, all of the bubbles are ejected into the liquid core, even those nucleating immediately after the ONB.

The photographic results show that all bubbles at low pressure detach from the heater immediately after the onset of nucleate boiling (Bibeau & Salcudean 1994), and not at the OSV, as stipulated by previous void growth models (Levy 1967; Staub 1968; Rogers *et al.* 1987). No region of "attached void" is observed before the onset of significant void at low pressure. It is therefore concluded that the onset of significant void is not related to bubble detachment.

The axial distance traversed by the bubbles digitized for conditions listed in table 3 from inception to collapse is 2.0 mm on average. These results were obtained for conditions before and after the OSV, but do not include bubbles nucleating close to the ONB where considerable sliding was observed, as reported in Bibeau & Salcudean (1994). From these results, it may be concluded that bubbles do not influence conditions far downstream; the influence of each bubble is locally confined to a small portion of the heater element.

The assumption that bubbles traveling in a bubble layer away from the wall become unstable and are ejected into the fluid core at the onset of significant void (Serizawa & Kenning 1979; Dix 1971), cannot be substantiated by this investigation for two reasons: (i) bubbles are ejected into the liquid core after the ONB, and not at the OSV; and (ii) there is no well-defined detached bubble layer in the highly subcooled region. High speed photography shows that, in the highly subcooled region, a bubble layer consisting of bubbles moving in the fluid core over long distances as described by Dix (1971) does not exist. Instead of a well-defined, detached bubble layer, the present photographic study reveals individual bubbles nucleating on the heated wall which slide on the wall before being ejected into the subcooled flow, where they condense rapidly. The residence time the bubble spends away from the wall is short, typically less than 1 ms, and therefore a layer of detached bubbles cannot be seen. In addition, the average axial translation of the bubbles after ejection is 0.6 mm on average. Even after the OSV, where many bubbles nucleate at the same time and then coalesce, the bubbles spend most of their life cycles sliding on the wall, and the residence time in the core of the flow is short in comparison.

The bubble detachment behavior for forced-convection subcooled boiling observed in the present photographic study differs from the observations reported by Klausner *et al.* (1993) for saturated boiling conditions. They report that bubbles either slide away from the nucleation site, or eject from the nucleation site into the flow (without prior sliding). The present measurements of the parallel displacement of the center of mass of the bubbles show that bubbles always slide along the heater before being ejected. This was also observed for a subcooling of 10°C which is near saturation conditions. Klausner *et al.* (1993) did not report measurements of the displacement of the center of mass of the bubble. Since the sliding of the bubble may be typically less than 2 mm for a flow velocity of 1.0 m/s, only an accurate measurement of the parallel displacement of the bubble can provide conclusive evidence on whether the bubble slides before ejection. Figure 13 provides experimental proof of the detachment mechanism in subcooled boiling: bubbles first slide away from the nucleation site at parallel detachment, and are then subsequently ejected into the flow at normal detachment.

6. VOID GROWTH MODELING

6.1. Summary of experimental findings

Void growth models (table 1), developed mainly for higher pressure applications than those addressed in this study, assume that the onset of significant void is governed either by (i) the location where fully developed nucleate boiling begins, (ii) the location where the bubbles first depart from the heater or (iii) the location where the bubbles are first ejected into the flow from a detached bubble layer. In addition, some models assume that the highly subcooled region corresponds to the attached void region, where void fraction is negligible, and that bubbles do not slide, but rather grow and collapse on the wall. Although these models have contributed significantly to the representation of void growth at elevated pressure, experimental evidence,

obtained from wall temperature measurements, void fraction measurements and a photographic study, shows that none of these assumptions is applicable to low pressure and low velocity conditions.

Simultaneous measurement of void fraction and wall temperatures shows that the OSV occurs in the fully developed nucleate boiling region. The OSV is not related to bubble detachment, since bubbles detach from the wall after the onset of nucleate boiling. The OSV is not determined by the location where the bubbles are first ejected from a detached bubble layer, since bubbles are ejected into the flow after the ONB. The experimental findings also show that bubbles slide away from their nucleation sites after nucleating (parallel detachment), and are later ejected into the flow (normal detachment). No region of "attached void" was observed before the OSV, and the void fraction may be as high as 10% at the OSV.

The assumptions which are commonly applied at high pressure in the description of bubble behavior and the prediction of void growth are not valid for the conditions of this study. To facilitate the understanding of void growth at low pressure and low velocity, a phenomenological void growth model has been developed based on the experimental findings obtained from the photographic study and void growth measurements.

6.2. Preliminary considerations

A phenomenological void growth model should be based on assumptions consistent with physical observations with each assumption being independently validated. This is necessary to avoid the dependence of the model performance on empirical constants rather than on a sound phenomenological understanding. For example, the bubble detachment model of Levy (1967) predicts void fraction measurements reasonably well at atmospheric pressure for the experimental investigations of Evangelisti & Lupoli (1968) and Edelman & Elias (1981), both investigations at atmospheric pressure and mass flux below 1500 kg/m^2 s. The Levy model, however, did not compare favorably with the void fraction measurements in Mcleod (1986) for a pressure of 1.5 bar. The assumption that the OSV occurs when the bubble first detaches from the wall was shown to be invalid at low pressure. The capacity of detachment-based models (Levy 1967) to occasionally predict void fraction reasonably well at low pressure may be attributed to the correlation of the low pressure data through empirical constants, rather than the validity of the assumptions.

Void growth models can be separated into two categories: "profile-fitting models", where the true mass fraction and the equilibrium quality at the OSV are fitted using an exponential function (Levy 1967; Bowring 1962), and "mechanistic models", where expressions for the production and condensation of vapor are generally developed by partitioning the heat flux at the wall into different components (Rouhani & Axelsson 1970).

Profile-fitting models predict void growth successfully at high pressure (Saha & Zuber 1974; Levy 1967). The success of these models may be attributed to the profile-fitting of the mass fraction, and to the fact the OSV is already well established by a correlation. It may be argued that some aspects of profile-fitting models are similar to correlating void fraction directly. In both cases, an exponential form is assumed, and empirical constants are evaluated, based on the void fraction data.

Mechanistic models assume the variation of certain parameters (e.g. the bubble agitation parameter, Bowring 1962) introduced during the modeling of void growth. The variation of these parameters is either assumed *a priori* or deduced from the void fraction experimental data. The independent variation of these parameters with pressure, heat flux and subcooling is not known. For example, the percentage of the surface influenced by single phase flow in Rouhani & Axelsson's model (1970) cannot be evaluated experimentally, the bubble agitation parameter in Bowring's model (1962) is evaluated from the void fraction data, and the bubble radius in Chatoorgoon's model (1992) is assumed constant (1.25 mm) for different values of heat flux, subcooling and pressure.

When developing a phenomenological void growth model, parameters should be evaluated either by independent experiments or by analysis. It should also be possible to vary these parameters independently of pressure, heat flux and local subcooling.

To take into account the various aspects of void growth modeling discussed above, it was considered necessary to develop a void growth model which depends upon parameters that could be analytically or experimentally evaluated, using the information on the bubble ebullition cycle obtained from the high speed photographic study.

6.3. Bubble accounting model

The bubble accounting model was developed based on the definition of the void fraction as the area occupied by the vapor divided by the cross-sectional area. For a boiling channel of arbitrary geometry, the void fraction is:

$$\epsilon = \frac{A_G}{A_c} \quad [4]$$

where A_G is the area occupied by the vapor at a cross-section of zero thickness of the boiling channel. In practice, the void fraction is measured within a control volume of finite thickness Δl. For small values of Δl, the void fraction defined within a control volume ϵ_{cv} is similar to ϵ, so that:

$$\epsilon = \epsilon_{cv} = \frac{A_G \Delta l}{A_c \Delta l} = \frac{V_{G_{cv}}}{A_c \Delta l} \quad [5]$$

where $V_{G_{cv}}$ is the volume of vapor inside the control volume. The volume of vapor in the control volume is equal to the product of the number of nucleation sites on the surface of the heater and the vapor contribution of each nucleating bubble during one bubble period, which includes the waiting time. This can be expressed as:

$$V_{G_{cv}} = (N_a P_h \Delta l)\left(\bar{V}_b \frac{t_b}{t_p}\right) \quad [6]$$

where

N_a = nucleation site density (bubbles/m^2)
P_h = heated perimeter of the heater (m)
$\bar{V}_b$ = average bubble volume produced by each nucleation site during life time t_b (m^3)
t_b = bubble life time from inception to collapse (s)
t_p = bubble period (s).

The convection of void can be neglected based on the results of the photographic study.

Using [5] and [6], the void fraction inside the control volume can be expressed as:

$$\epsilon = \frac{P_h}{A_c} N_a \bar{V}_b \frac{t_b}{t_p} \quad [7]$$

The average volume equivalent radius, $\bar{R}_b$, is related by definition to the average bubble volume, $\bar{V}_b$ as follows:

$$\bar{V}_b = \tfrac{4}{3}\pi \bar{R}_b^3 \quad [8]$$

and the average bubble frequency, f, equals the inverse of the time period, t_p. Using these two definitions, the void fraction can be expressed as:

$$\epsilon = \left(\frac{4\pi P_h}{3A_c}\right)(N_a f)(\bar{R}_b^3 t_b) \quad [9]$$

It has been shown experimentally (Jacob & Linke 1949; Hatton & Hall 1966) that the frequency of bubble generation is dependent upon the bubble departure diameter in nucleate boiling. Ivey (1967) has shown that the frequency to bubble departure diameter relationship is dependent upon the bubble growth regime: for the dynamically controlled region,

$$f D_d^{0.5} = c_1 \quad [10]$$

and for the thermally controlled region,

$$f D_d^2 = c_2 \quad [11]$$

In order to assess whether the bubble growth rate is dynamically or thermally controlled, the bubble growth rate is compared to bubble growth rate predictions from the literature for bubbles growing in a uniform temperature field with no cross-flow. It is assumed that the main flow velocity and the temperature gradient do not affect significantly whether the growth rate is dynamically or thermally controlled. For a bubble growing on the wall, the dynamically controlled Rayleigh solution (Mikic 1970) is:

$$r_b = At \qquad [12]$$

where

$$A = \left[\frac{(\pi/7)h_{fG}\rho_G(T_w - T_{sat})}{\rho_L T_{sat}}\right]^{1/2} \qquad [13]$$

For the thermally controlled region, the Plesset solution (Mikic 1970) is:

$$r_b = Bt^{1/2} \qquad [14]$$

where

$$B = \left(\frac{12\mathrm{Ja}_w^2 a_L}{\pi}\right)^{1/2} \qquad [15]$$

and a_L is the liquid thermal diffusivity and Ja_w is defined in [21].

Figure 14 shows the comparison between the bubble ebullition cycle for the bubble sliding phase (obtained from high speed photography), the bubble growth rate prediction for the dynamically controlled region (Rayleigh solution), and the thermally controlled region (Plesset solution), for $T_{sub} = 30°C$, $\phi = 0.5\ \mathrm{MW/m^2}$ and $U = 0.82$ m/s. The experimental bubble growth rate results (the region between $0 < t < 0.7$ ms) lie closer to the Plesset solution, and, therefore, bubble growth can be assumed to be thermally controlled, and the frequency can be related to the bubble diameter at detachment by [11].

The frequency is assumed to vary inversely with the square of the average volume equivalent radius, instead of the bubble diameter at detachment, as follows:

$$f\overline{R}_b^2 = C_f \qquad [16]$$

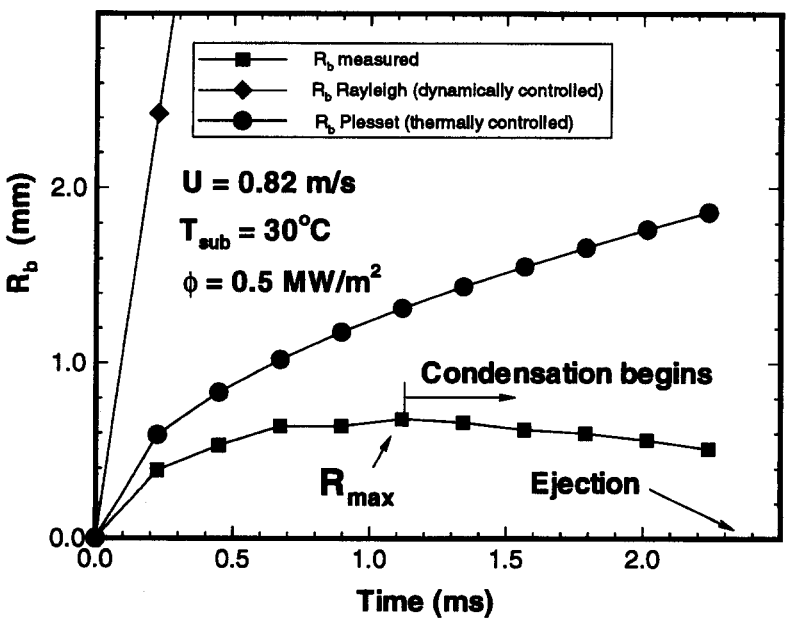

Figure 14. Comparison of the bubble ebullition cycle with the bubble growth rate prediction of the Rayleigh equation (dynamically controlled) and the Plesset equation (thermally controlled).

where C_f is a constant. The void fraction [9] can therefore be expressed as:

$$\epsilon = \left(\frac{4\pi P_h C_f}{3A_c}\right) N_a (\bar{R}_b t_b) \qquad [17]$$

Since the average volume equivalent radius, $\bar{R}_b$, is not a common characteristic parameter used in nucleate boiling studies, it will be replaced in the following section with a different variable.

6.4. Bubble cycle characteristic parameters

In nucleate boiling and void growth studies, the bubble diameter at departure is extensively used to characterize the bubble ebullition cycle (Levy 1967; Ivey 1967), and there is no reference to the maximum diameter. This is based on the premise that these two diameters are identical in nucleate boiling under all conditions. For saturated boiling conditions, the maximum bubble diameter and the bubble diameter at departure may be identical. In forced-convective subcooled nucleate boiling, the bubble diameter at departure (normal detachment) is smaller than the maximum bubble diameter, as shown in figure 13. It is therefore suggested that the bubble diameter at departure is not necessarily the best parameter for characterizing the ebullition cycle. The bubble shape at the point of departure is elongated and distorted by the thermal gradients, with the result that this diameter is not well defined. Therefore, the use of the diameter at departure is inappropriate when characterizing the bubble life cycle for conditions of subcooled nucleate boiling.

Conversely, the maximum bubble radius occurs during the early stage of the bubble life cycle, when the bubble is nearly spherical and therefore easier to define experimentally. The use of the maximum radius is also supported by the fact that the amount of fluid disturbed, the area of bubble influence, and the disturbance of the thermal layer are all proportional to the maximum bubble radius. These observations lead to the conclusion that the maximum diameter (or radius) should be used for subcooled nucleate boiling conditions.

It is possible to substitute R_{max} for $\bar{R}_b$ in [17] by changing the product $\bar{R}_b t_b$ to $R_{max} t_c$ in the bubble accounting model [17]. Figure 15(a) shows that the area under the R_b curve, from inception to complete condensation, can be represented by the rectangular area formed by $\bar{R}_b t_b$. This area is approximated by the rectangular area bounded by $R_{max} t_c$, as shown in figure 15(b). Figure 16 compares the areas bounded by $\bar{R}_b t_b$ and $R_{max} t_c$, for subcoolings between 10 and 40°C. The results

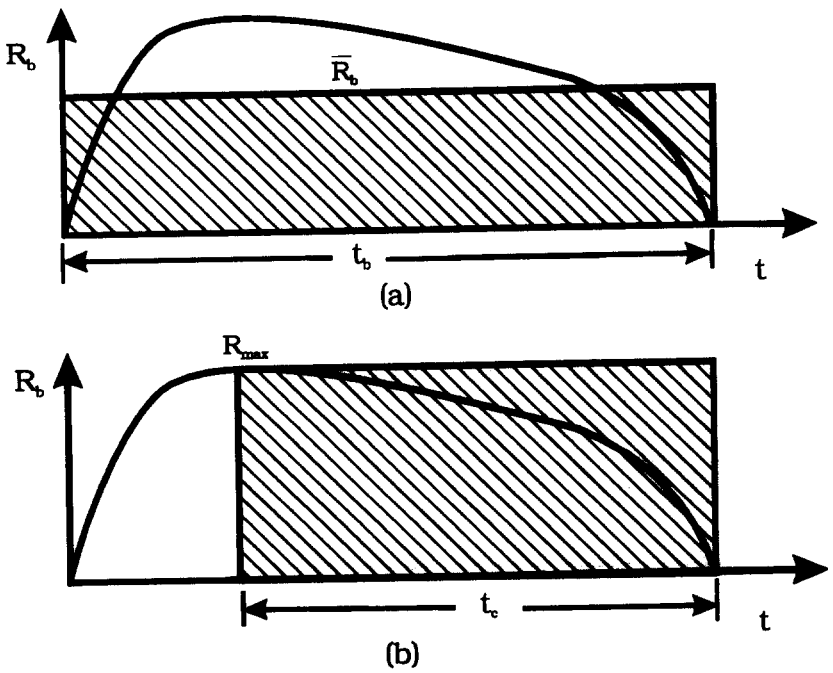

Figure 15. Area under the volume equivalent radius (a) $\bar{R}_b t_b$ and (b) $R_{max} t_c$.

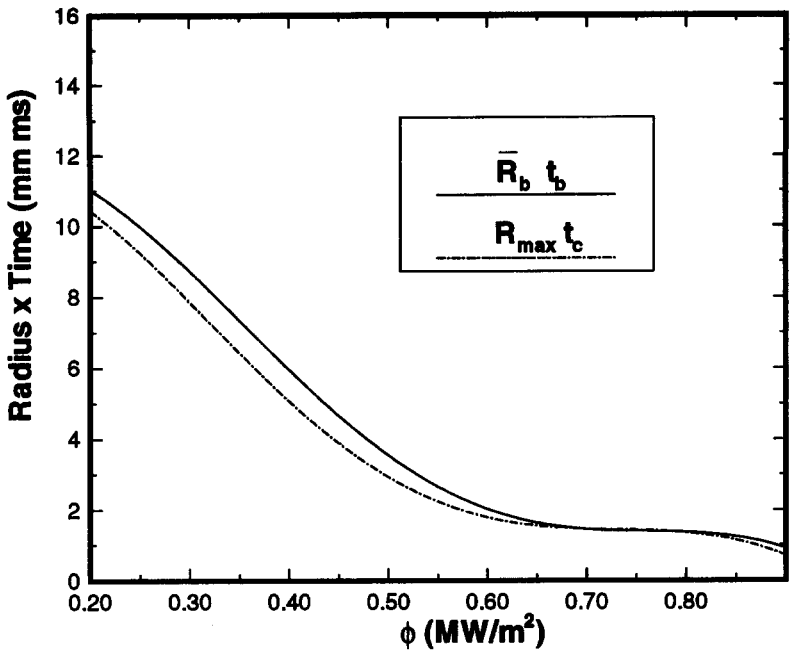

Figure 16. Comparison between area bounded by $\bar{R}_b t_b$ and $R_{max} t_c$.

show that the two areas are similar, especially at heat fluxes greater than 0.6 MW/m^2. The product $\bar{R}_b t_b$ in the bubble accounting model can therefore be approximated by $R_{max} t_c$. The area bounded by $\bar{R}_b t_b$ is at its maximum at low heat fluxes, and becomes nearly constant at heat fluxes above 0.6 MW/m^2. This approximation is only possible if the bubbles condense in the liquid after being ejected, and is justified for subcooled boiling conditions, since bubbles in the liquid core do not grow, as observed experimentally.

The substitution of t_c for t_b in [17] is also more convenient, as the bubble life time, t_b, depends on the bubble condensation time, t_c, as well as the bubble growth time, t_g.

After substituting the bubble characteristic parameters $R_{max} t_c$ for $\bar{R}_b t_b$ in [17], the void fraction data can be written as:

$$\epsilon = \left(\frac{4\pi P_h C_f}{3A_c}\right) N_a R_{max} t_c \qquad [18]$$

which depends upon the nucleation site density, the maximum radius and the condensation time, all of which vary with subcooling, heat flux and pressure.

6.5. Model evaluation

Based on the analysis of the high speed photographic films obtained in this study, the maximum radius, R_{max}, is obtained from the following correlation developed by Farajisarir (1993):

$$K_\sigma = 5.01 \times 10^9 (\mathrm{Ja}_w \vartheta)^{-1.65} \qquad [19]$$

where the surface tension number, the Jacob number based on the wall temperature and the subcooling parameter are, respectively:

$$K_\sigma = \frac{R_{max}\sigma}{\rho a_L^2} \qquad [20]$$

$$\mathrm{Ja}_w = \frac{\rho_L C_p (T_w - T_{sat})}{\rho_G h_{fG}} \qquad [21]$$

$$\vartheta = \frac{T_w - T_b}{T_w - T_{sat}} \qquad [22]$$

Equation [19] predicts that an increase in the heat flux, which causes the Jacob number Ja_w to increase, decreases the maximum diameter for constant subcooling. This is consistent with experimental findings which show bubbles becoming smaller as the heat flux is increased at constant subcooling due to nucleation site interactions. An increase in the subcooling causes an increase in the parameter ϑ, which results in a decrease of the maximum radius due to greater heat loss around the bubble. The main flow velocity does not have a direct effect on the maximum radius, since the slip ratio is approx. 1. Convection effects are therefore minimized, but the flow velocity may affect the maximim bubble radius indirectly through the wall superheat.

The condensation time, t_c, is also obtained from the photographic study. Farajisarir (1993) developed a correlation for the condensation time as:

$$t_c^+ = 106.8 Ja_b^{-0.45} K_\sigma^{1.30} \quad [23]$$

where

$$t_c^+ = \frac{a_L t_c}{\left(\frac{\rho_L \sigma_L^2}{\sigma}\right)^2} \quad [24]$$

$$Ja_b = \frac{\rho_L C_p (T_{sat} - T_b)}{\rho_G h_{fG}} \quad [25]$$

Unlike the definition of the condensation time in the literature, the condensation time in this study is defined as the interval between the time when the bubble reaches R_{max} to the time when the bubble has fully condensed in the fluid core. Equation [23] shows that the condensation time is dependent upon the maximum radius, and increases as the maximum bubble radius increases. The dependence of condensation time on the maximum radius implies that t_c decreases with increasing heat flux at constant subcooling. The condensation time increases as the subcooling decreases, since the heat transfer from the bubble to the surrounding liquid is dependent upon the degree of subcooling.

The nucleation site density is obtained from the pool boiling correlation developed by Kocamustafaogullari & Ishii (1983), which was derived for pressures between 1 and 147 bar. The correlation is expressed as:

$$N_a^* = f(\rho^*) R_c^{*-4.4} \quad [26]$$

where the dimensionless nucleation site density and the dimensionless cavity size are defined as:

$$N_a^* = N_a D_{df}^2 \quad [27]$$

$$R_c^* = \frac{2R_c}{D_{df}} \quad [28]$$

where R_c is the cavity radius and D_{df} is the Fritz bubble diameter at detachment, calculated by the modified Fritz correlation (Kocamustafaogullari & Ishii 1983):

$$D_{df} = 0.0208\theta \sqrt{\frac{\sigma}{g(\rho_L - \rho_G)}} \quad [29]$$

where θ is the equilibrium contact angle.

To be consistent with the model developed by Kocamustafaogullari and Ishii, the Fritz bubble detachment diameter, D_{df}, is used instead of D_{max}. The Fritz bubble detachment diameter does not have a physical meaning in the context of the bubble accounting model because, for a vertical channel, there is no buoyancy force normal to the heater. Therefore, the Fritz bubble detachment diameter is used only to non-dimensionalize the nucleation site density. The equilibrium angle was set to 60°, since this value was found to correspond to Ishii's correlation for water at atmospheric pressure. The cavity radius is expressed as:

$$R_c = \frac{2.0\sigma\left(1 + \frac{\rho_G}{\rho_L}\right)}{P} \left[e^{(h_{fG}(T_G - T_{sat})/RT_G T_{sat})} - 1\right]^{-1} \quad [30]$$

where R is the ideal gas constant, and T_G is the temperature of the vapor inside the bubble. The pressure dependent function is:

$$f(\rho^*) = 2.157 \times 10^{-7}\rho^{*-3.2}(1 + 0.0049)\rho^*)^{4.13} \quad [31]$$

where $\rho^* = (\rho_L - \rho_G)/\rho_G$.

The constant C_f in [16] can be evaluated from the photographic films. Ten films were analyzed for different conditions, and the bubble frequency was evaluated for at least ten bubbles at each condition. A single frequency was obtained for each condition by averaging the evaluated frequencies. The average equivalent volume radius, $\bar{R}_b$, was then calculated for each condition. The constant C_f was determined using [16], and the value obtained from the analysis of the films was 0.000057 m^2/s.

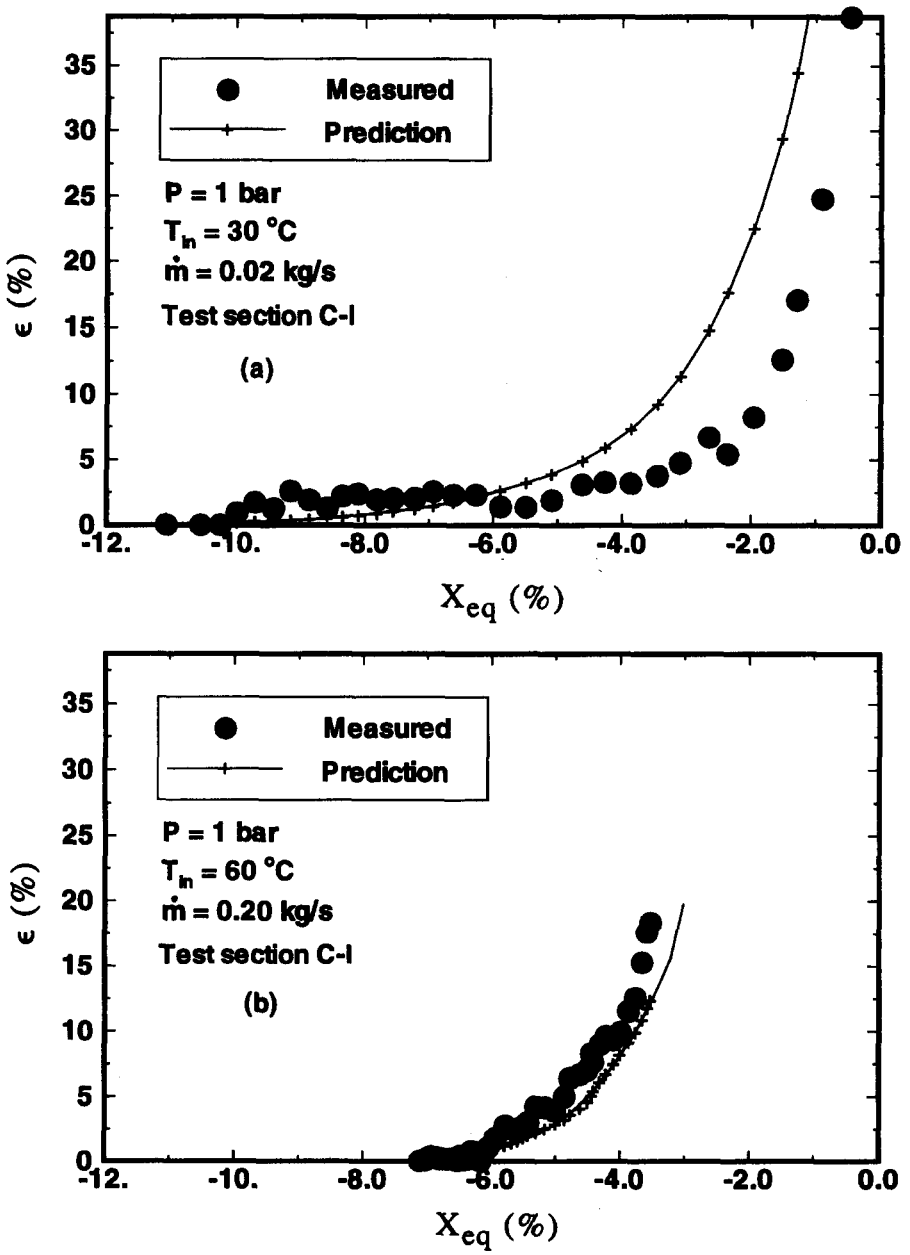

Figure 17. Bubble accounting model prediction compared with experimental results for experiments.

The wall temperature required for the evaluation of R_c and Ja_w was evaluated using the Shah correlation (Shah 1983), developed for subcooled boiling conditions. This correlation was found to predict accurately the wall temperature measurements for test section C-1 (Bibeau 1988).

The bubble accounting model [18] is compared to the void fraction measurements at atmospheric pressure for test section C-1 in figures 17(a) and (b) for flow rates of 0.02 and 0.20 kg/s, respectively. The results are scaled with the equilibrium quality. The model predicts the void fraction satisfactorily, considering none of the coefficients were optimized based on the void growth data. A method for calculating the error is introduced below.

The average void fraction error, ϵ_{err}, between the measured and predicted values is defined as:

$$\epsilon_{err} = \frac{\sum_{i=1}^{n} |(\epsilon_m - \epsilon_p)|}{n} \quad [32]$$

where n equals the number of void fraction measurements, ϵ_m the measured void fraction, and ϵ_p the predicted void fraction. The measurement error for ϵ_m is $\pm 3\%$ void, while the error for the scaling parameter X_{eq} varies from 0.1 to 0.5% quality, depending upon the input parameters: P, T_{in}, $\dot{m}$ and ϕ. The permissible error between the predicted void fraction and the measured void fraction is $\delta\epsilon$, and varies depending on the slope of the void growth curve. In the highly subcooled region, void fraction is fairly insensitive to changes in X_{eq}, so $\delta\epsilon = \pm 3\%$. In the exponential region, void fraction is very sensitive to small changes in X_{eq}, which are of the same order of magnitude as the measurement error of X_{eq}. Therefore, $\delta\epsilon$ in this region is also a function of the slope of the void growth curve, and may be higher than 10% void. Since $\delta\epsilon$ is smaller in the highly subcooled region than in the exponential region, the void fraction error decreases if more measurements are obtained in the highly subcooled region than in the exponential region. The average void fraction error is therefore dependent on the ratio of data points obtained in the highly subcooled region to the data points obtained in the exponential region.

A method to quantify the model prediction error is proposed. The void fraction error in the exponential region is multiplied by weight factors of 1, 5 and 10 for void fraction values greater than 15% void (exponential region). In this manner, void fraction error measured with a weight factor of 1 reflects the accuracy of the prediction of the correlation in the highly subcooled region, while weight factors of 5 and 10 reflect the accuracy in the exponential region. This method ensures that the evaluation of the model error is not biased by having more experimental data points in the highly subcooled region. The weighted void fraction error between model prediction and void fraction measurements (580 data points for test section C-1 at atmospheric pressure) is:

Weight	ϵ_{err} (% void)
1	2.8
5	4.3
10	5.4

6.6. Model performance

Figure 18(a)–(c) shows the variation of six parameters evaluated by the bubble accounting model [for the same conditions as in figure 17(a)]: maximum radius, R_{max}, condensation time, t_c, nucleation site density, N_a, cavity size, R_c, frequency, f, and the ratio of the bubble spacing to the maximum diameter, s_p/D_{max}. Results are scaled with the equilibrium quality, X_{eq}.

Figure 18(a) shows that the maximum radius and the condensation time increase with increasing equilibrium quality. In some cases, the model predicted that the maximum bubble radius would initially decrease at high subcoolings, and subsequently increase at low and medium subcoolings, since two opposing trends appear as the equilibrium quality increases. The equilibrium quality increases due to a decrease in subcooling, which increases the bubble radius. The equilibrium quality also increases due to an increase in heat flux, which decreases the bubble radius.

Figure 18(b) shows that the nucleation site density increases from 0.05×10^6 to $4.0 \times 10^6\ m^{-2}$ with increasing equilibrium quality. The figure also shows the critical cavity radius, which decreases from 1.2 to 0.6 μm with increasing equilibrium quality.

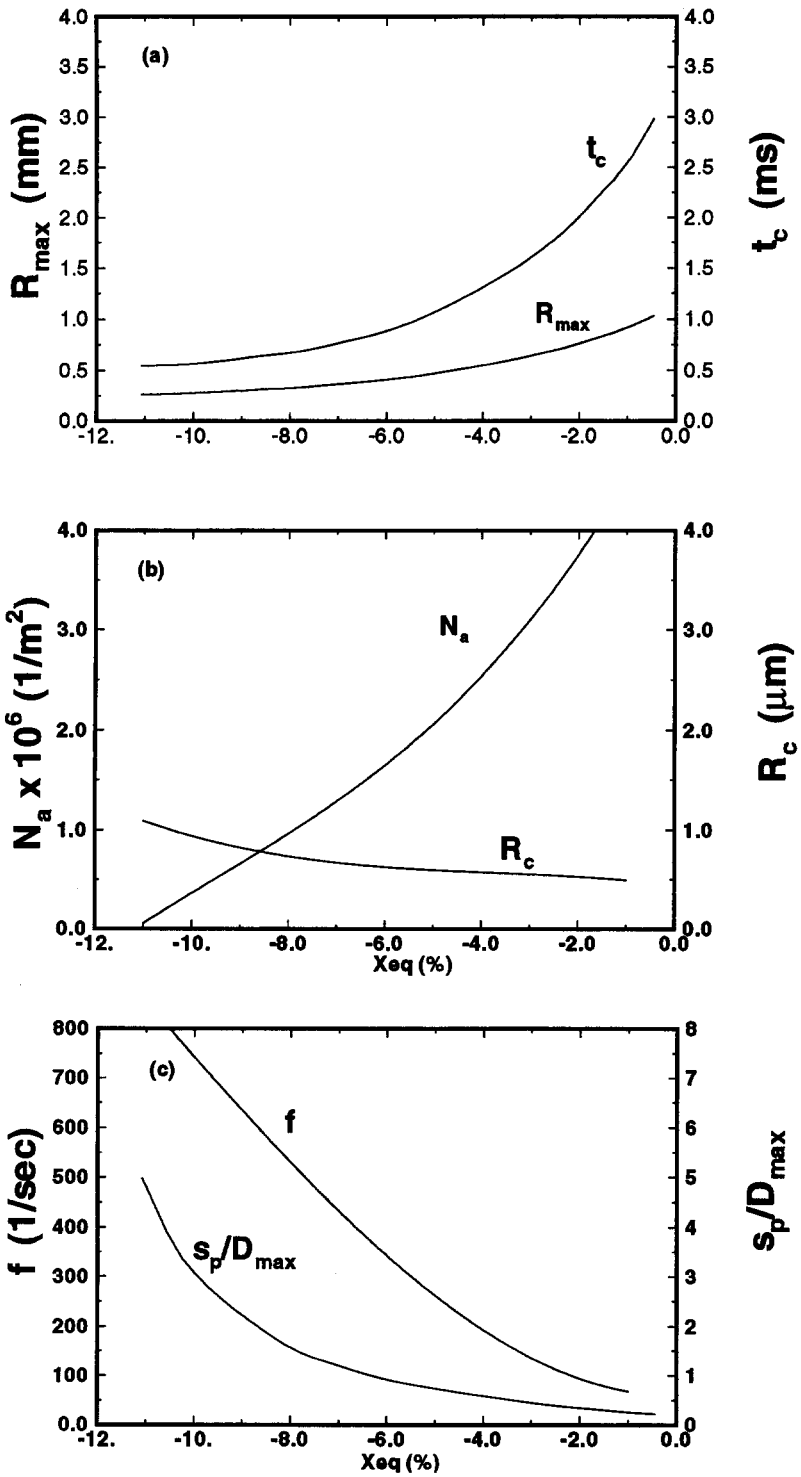

Figure 18. Variation of the parameters used in the evaluation of the bubble accounting model for $P = 1$ bar, $T_{in} = 30°C$, $\dot{m} = 0.02$ kg/s and test section C-1: (a) maximum bubble radius and condensation time, (b) nucleation site density and critical cavity size and (c) frequency and bubble spacing to maximum diameter ratio.

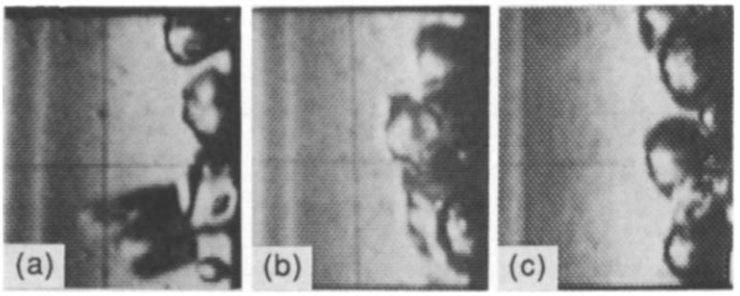

Figure 19. Bubble crowding near the onset of significant void for conditions: (a) $\phi = 0.4\,\mathrm{MW/m^2}$, $\dot{m} = 0.10\,\mathrm{kg/s}$ and $T_{sub} = 10^{\circ}\mathrm{C}$, (b) $\phi = 0.9\,\mathrm{MW/m^2}$, $\dot{m} = 0.20\,\mathrm{kg/s}$ and $T_{sub} = 20^{\circ}\mathrm{C}$ and (c) $\phi = 0.9\,\mathrm{MW/m^2}$, $\dot{m} = 0.10\,\mathrm{kg/s}$ and $T_{sub} = 20^{\circ}\mathrm{C}$.

Figure 18(c) shows that the frequency of bubble nucleation decreases with increasing equilibrium quality, due to the increase in the maximum bubble radius. The bubble frequency varies with heat flux and subcooling, since it is dependent upon the maximum bubble radius. An increase in the maximum bubble radius increases the condensation time and decreases the bubble frequency, which is in accordance with the high speed photographic study. The figure also shows the bubble spacing to maximum diameter ratio, which reflects the crowding of the bubbles. Bubble coalescence may occur when†:

$$\frac{s_p}{D_{max}} < 1 \qquad [33]$$

The model shows coalescence may begin before the OSV ($X_{eq_{osv}} = -2.8\%$), which is consistent with observations made from the high speed photographic films.

Figure 19(a)–(c) shows typical bubble crowding on the surface after the OSV for different conditions. Bubbles are observed to coalesce on the wall and then eject together into the flow.

6.7. Model characteristics

The bubble accounting model evaluates the production of vapor at the heated wall, which is governed by the wall superheat. In the highly subcooled region, the bubble radius and the condensation time are small, and therefore, the void fraction is low. As the equilibrium quality increases, the maximum bubble radius does not increase significantly in the highly subcooled region. This behavior is due to the two opposing trends associated with increasing equilibrium quality [see figure 18(a)]: the decrease in the bubble radius with increasing heat flux, and the increase in bubble radius with decreasing subcooling. The present bubble accounting void growth model is the first to predict a diminishing bubble radius as the heat flux is increased at constant subcooling.

The OSV is governed by the increase in bubble production and the bubble condensation time. The increase in bubble production is due to the increase in bubble radius and in the number of nucleation sites; the increase in bubble condensation time is due to an increase in the bubble radius and a decrease in the subcooling. A longer condensation time implies that each bubble produced on the heated wall contributes to void production over a longer time period. The OSV is not governed by bubble coalescence since bubble coalescence can also be observed in the highly subcooled region.

The prediction of void growth using the bubble accounting model provides a better understanding of the influence of input parameters (ϕ, T_{in} and $\dot{m}$) on void fraction for subcooled boiling applications at low pressure. The onset of significant void is not required, and there are no empirical constants tuned to the experimental data. The accuracy of the model, therefore, can be somewhat lower. The present model was developed for atmospheric pressure since the maximum radius and condensation time were obtained at atmospheric pressure. The bubble radius is influenced by pressure variation between 1 and 3 bar (Bibeau & Salcudean 1994), so other expressions for the

†Bubble coalescence would occur at $s_p/D_{max} = 1$ only if there was no waiting time between bubble ebullition cycles. This situation does not occur.

maximum radius and condensation time must be used at pressures greater than 1 bar. These expressions depend upon the thermalhydraulic conditions involved. Recent trends in the literature (Del Vale & Kenning 1985; Shoukri *et al.* 1990) show that nucleate boiling studies investigate the ebullition cycle in more detail, suggesting that more general correlations and analytical models will be developed in the future. The development of digitizing technology and high speed video cameras will help improve the future of void growth models based on the principles of the bubble accounting model.

7. CONCLUSIONS

Void fraction, wall temperature measurements and high speed photographic results provide the following experimental evidence:

(1) Wall temperature measurements show that the OSV is not governed by the transition between partially-developed boiling and fully-developed boiling.
(2) Without exception, bubbles slide on the wall after nucleating, and subsequently are ejected into the flow. There is no region where bubbles grow and collapse on the wall, nor is there a region of attached void.
(3) The OSV does not occur at bubble detachment, as is assumed in most void growth studies, since the bubbles detach from the heater immediately after the ONB.
(4) The OSV does not occur when the bubbles are first ejected into the flow, since the bubbles are ejected immediately after ONB.
(5) There is no layer of detached bubbles in the highly subcooled region, since bubbles condense rapidly: the bubbles travel downstream less than 1 bubble diameter after ejection.
(6) Void fraction in the highly subcooled region is important, and may be as high as 10% at low flow rates.
(7) Bubbles nucleating on the heater do not influence conditions far downstream, since the total axial distance traveled by the bubbles is typically less than 2 mm.
(8) Bubbles condense significantly while sliding on the wall.

A phenomenological void growth model was developed, based on an accounting of the vapor volume inside a heated channel for subcooled conditions at atmospheric pressure. The void depends upon the nucleation site density, the maximum radius, and the condensation time as follows:

$$\epsilon = \left(\frac{4\pi P_h C_f}{3A_c}\right) N_a R_{max} t_c. \qquad [34]$$

All the parameters used in the bubble accounting model (R_{max}, t_c and N_a) vary independently with heat flux and subcooling, and assumptions are based on experimental evidence. The empirical coefficients in the bubble accounting model are neither determined nor optimized from the void fraction experimental data. The bubble accounting model predicts void fraction for the large circular test section with an error of 2.8% void; when the void fraction error in the exponential region is weighted with a value of 10, the error is 5.4% void.

Acknowledgements—We would like to thank D. Farajisarir for his contribution in developing the high speed photographic and digital analysis experimental setup. The discussions with Dr Yacov Barnea during this investigation are gratefully acknowledged. We acknowledge Deborah Varley's careful editing. The work was funded by the Natural Sciences and Engineering Research Council of Canada and by Atomic Energy of Canada Limited.

REFERENCES

AHMAD, S. Y. 1970 Axial distribution of bulk temperature and void fraction in a heated channel with inlet subcooling. *J. Heat Transfer* 595–608.

AKIYAMA, M. & TACHIBANA, F. 1974 Motion of vapor bubbles in subcooled heated channel. *Bull. JSME* **17**, 241–247.

BIBEAU, E. L. 1988 Experimental investigation of subcooled void growth for upflow and downflow at low velocities and low pressure. M.Sc. thesis, University of British Columbia.

BIBEAU, E. L. 1993 Void growth in subcooled flow boiling for circular and finned geometries for low values of pressure and velocity. Ph.D. thesis, University of British Columbia.

BIBEAU, E. L. & SALCUDEAN, M. 1990 The effect of flow direction on void growth at low velocities and low pressure. *Int. Comm. Heat Mass Transfer* **17,** 19–25.

BIBEAU, E. L. & SALCUDEAN, M. 1994 A study of bubble ebullition in forced-convective subcooled nucleate boiling at low pressure. *Int. J. Heat Mass Transfer*. In press.

BIBEAU, E. L., SALCUDEAN, M. & KOWALSKI, J. E. 1993 Subcooled void growth for finned and annular geometries at low velocities and low pressures. *Third World Conference on Experimental Heat Transfer, Fluid Mechanics and Thermodynamics*, Hawaii.

BOWRING, R. W. 1962 Physical model based on bubble detachment, and calculation of steam voidage in the subcooled region of a heated channel. HPR-29, Institutt for Atomenergi, Halden, Norway.

CHANG, YAN-PO 1963 Some possible critical conditions in nucleate boiling. *J. Heat Transfer* **85,** 89–100.

CHATOORGOON, V. 1992 A generation–condensation void transport model for low pressure. AECL Publication.

DIX, G. E. 1971 Vapor void fraction for forced convection with subcooled boiling at low flow rates. Ph.D. thesis, University of California, Berkeley, CA.

EDELMAN, Z. & ELIAS, E. 1981 Void fraction in low flow rate subcooled boiling. *Nuclear Engng Design* **63,** 375–382.

EVANGELISTI, R. & LUPOLI, P. 1968 The void fraction in an annular channel at atmospheric pressure. *Int. J. Heat Mass Transfer* **12,** 699–711.

FARAJISARIR, D. 1993 Bubble dynamics in subcooled flow boiling. M.Sc. thesis, University of British Columbia.

GRIFFITH, P., CLARK, J. A. & ROHSENOW, W. W. 1985 Void volumes in subcooled boiling systems. *Trans. ASME*, paper 58-HT-19.

GUNTHER, F. C. 1951 Photographic study of surface-boiling heat transfer to water with forced convection. *Trans. ASME* **73,** 115–123.

HATTON, A. P. & HALL, I. S. 1966 Photographic study of boiling on prepared surfaces. *Third International Heat Transfer Conference*, Chicago, IL, paper 115, pp. 24–31.

HILBORN, J. W., KAY, R. E., STEVENS-GUILLE, P. D. & JERVIS, R. E. 1972 SLOWPOKE at the University of Toronto—a laboratory reactor for neutron irradiation. Atomic Energy of Canada Limited, Chalk River, Ontario.

HSU, Y. Y. & GRAHAM, R. W. 1961 An analytical and experimental study of the thermal boundary layer and ebullition cycle in nucleate boiling. NA. . Technical Note D-594.

IVEY, H. J. 1967 Relationships between bubble frequency, departure diameter and rise velocity in nucleate boiling. *Int. J. Heat Mass Transfer* **10,** 1023–1040.

JACOB, M. & LINKE, W. 1949 *Heat Transfer*, Vol. 1. Wiley, New York.

KOCAMUSTAFAOGULLARI, G. & ISHII, M. 1983 Interfacial area and nucleation site density in boiling systems. *Int. J. Heat Mass Transfer* **26,** 1377–1387.

KOWALSKI, J. E., LIM, I. C. & HEMBROFF, R. L. 1988 Heat transfer in boiling of subcooled water on a finned tube. *5th Int. Symp. on Multi-phase Transport and Particulate Phenomena*, Miami, FL.

LAHEY, R. T. 1978 A mechanistic subcooled boiling model. *Sixth International Heat Transfer Conference*, Toronto, Canada, Vol. 1, pp. 293–297.

LARSEN, P. S. & TONG, L. S. 1969 Void fraction in subcooled flow boiling. *J. Heat Transfer* **91,** 471–476.

LEVY, S. 1967 Forced convection subcooled boiling—prediction of vapor volumetric fraction. *Int. J. Heat Mass Transfer* **10,** 951–965.

LIDSTONE, R. F. & SAROUDIS, J. I. 1986 MAPLE: a new multipurpose reactor for nuclear development in the 1990s. *Proceedings of Int. Symposium on the Significance and Impact of Nuclear Research in Developing Countries*, IAEA-SM-291/19, Athena's, Greece.

MCLEOD, R. D. 1986 Investigation of subcooled void fraction growth in water under low pressure and low flow rate conditions. M.Sc. thesis, Carleton University, Ottawa.

MIKIC, B. B., ROHSENOW, W. M. & GRIFFITH, P. 1970 On bubble growth rates. *Int. J. Heat Mass Transfer* **13,** 657–666.

ROGERS, J. T., SALCUDEAN, M., ABDULLAH, Z., MCLEOD, D. & POIRIER, D. 1987 The onset of significant void in upflow boiling of water at low pressure and velocities. *Int. J. Heat Mass Transfer* **30,** 2247–2260.

ROHSENOW, W. M. & CLARK, J. A. 1951 A study of the mechanism of boiling heat transfer. *Trans. ASME* 609–620.

ROUHANI, S. Z. 1968 Calculation of steam volume fraction in subcooled boiling. *J. Heat Transfer* **90,** 158–163.

SAHA, P. & ZUBER, N. 1974 Point of net vapor generation and vapor void fraction in subcooled boiling. *Int. Heat Transfer Conf., 5th, Proc.*, Tokyo, Japan, Vol. 4, Paper B4.7.

SALCUDEAN, M. & BIBEAU, E. L. 1991 Experimental investigation of flow direction effect on void growth at low velocities and low pressure. *Second World Conference on Experimental Heat Transfer, Fluid Mechanics and Thermodynamics*, Yugoslavia.

SERIZAWA, A. & KENNING, D. B. R. 1979 A study of forced convective subcooled flow boiling. Tech. Rep., Inst. Atomic Energy, Kyoto University.

SHAH, M. M. 1983 Generalized prediction of heat transfer during subcooled boiling in annuli. *Heat Transfer Engng* **4,** 24–31.

SHOUKRI, M., DONEVSKI, B., JUDD, R. L. & DIMMICK, G. R. 1990 Experimental on subcooled flow boiling and condensation in vertical annular channels. *International Conference in Multiphase Flow*, Dubrovnik, Yugoslavia.

STAUB, F. W. 1968 The void fraction in subcooled boiling—prediction of the initial point of net vapor generation. *J. Heat Transfer* **90,** 151–157.

UNAL, H. C. 1975 Determination of the initial point of net vapor generation in flow boiling systems. *Int. J. Heat Mass Transfer* **18,** 1095–1099.

UNAL, H. C. 1976 Maximum bubble diameter, maximum bubble-growth time and bubble-growth rate during the subcooled nucleate flow boiling of water up to 17.7 MN/m^2. *Int. J. Heat Mass Transfer* **19,** 643–649.